An EXAFS and HR-XANES study of the uranyl peroxides $[UO_2(\eta^2\text{-}O_2)(H_2O)_2]\cdot nH_2O$ (n = 0, 2) and uranyl (oxy)hydroxide $[(UO_2)_4O(OH)_6]\cdot 6H_2O$†

Aurora Walshe,[a] Tim Prüßmann,[b] Tonya Vitova*[b] and Robert J. Baker*[a]

The solid-sate structures of the two uranyl peroxides studtite, $[UO_2(\eta^2\text{-}O_2)(H_2O)_2]\cdot 2H_2O$, and metastudtite $[UO_2(\eta^2\text{-}O_2)(H_2O)_2]$ have been determined by U–L_3 edge extended X-ray absorption fine structure (EXAFS) spectroscopy and show that upon removal of the interstitial water in studtite there are structural changes with a small shortening of the $U\text{–}O_{peroxo}$ and small lengthening of the $U\text{–}O_{yl}$ bonds. High-energy resolution X-Ray absorption near edge structure (HR-XANES) spectroscopy has been used to probe the differences in the local electronic structure and, supported by *ab initio FEFF9.5.1* calculations, dehydration causes a shift to higher energies of the occupied O p-DOS and U d- and f-DOS of meta-studtite. The HR-XANES spectrum of schoepite, $[(UO_2)_4O(OH)_6]\cdot 6H_2O$, has been measured as the White Line intensity can give information on the mixing of metal and ligand atomic orbitals. There is an indication for higher degree of ionicity for the U–OH bond in schoepite compared to the $U\text{–}O_2$ bond in studtite.

Introduction

The safe stewardship of both legacy, current and future nuclear waste is one of the most important concerns for all countries that generate electricity from nuclear fission. Given the long half-lives and high specific activities of the trans-uranic elements, particularly Np, Pu, Am and Cm, long term storage represents a significant technical challenge. One method that is currently favoured by the EU is the storage in a geological repository.[1] The majority of spent nuclear fuel (SNF) contains UO_2, which under moist oxidising repository conditions is thermodynamically unstable and will oxidise to UO_3 *via* a number of phase-altered materials.[2] In tests on actual SNF[3] and surrogate UO_2,[4] a number of these phases have been identified. However, these phases are also susceptible to further reactivity for example, schoepite $[(UO_2)_4O(OH)_6]\cdot 6H_2O$ and its dehydrated congener metaschoepite $[(UO_2)_4O(OH)_6]\cdot 5H_2O$ are found to be replaced by studtite, $[(UO_2)(\eta^2\text{-}O_2)(H_2O)_2]\cdot 2H_2O$, over the course of two years in deionized water.[5] Further work have shown that studtite, and its dehydration product metastudtite $[(UO_2)(\eta^2\text{-}O_2)(H_2O)_2]$, can be formed by dissolution of UO_2,[6] or the phase-altered materials,[7] in the presence of H_2O_2. Studtite has also been characterised on the surface of SNF,[8] 'lava' from the Chernobyl Nuclear Plant accident,[9] and in naturally occurring uranium ores.[10] Moreover, under alkaline conditions different behaviour results and spectroscopic and structural studies have shown that peroxides can displace carbonate ligands[11] from aqueous $[UO_2(CO_3)_3]^{4-}$ to form $[UO_2(O_2)(CO_3)_2]^{4-}$ and in the presence of hydroxide ions at pH = 12, spectroscopic evidence for $[UO_2(O_2)(OH)_2]^{2-}$ and $[UO_2(O_2)_2(OH)_2]^{4-}$ has been presented.[12] At a pH range of 9.5 to 11.5, $[UO_2(O_2)(OH)]^-$ and $[(UO_2)_2(O_2)(OH)]^-$ were identified.[13] Two lithium salts of $[UO_2(O_2)_3]^{4-}$ have also been structurally characterised.[14] Perhaps most spectacularly, under alkaline conditions uranyl peroxides can self-assemble into nano-sized clusters[15] that have also been implicated as uranium speciation products in the crippled reactors in the Fukushima-Daiichi power plant.[16] Clearly the coordination chemistry of uranyl peroxides is developing rapidly and has relevance to environmental applications as well as fundamental uranyl chemistry.

The formation of studtite on SNF has been ascribed to the production of H_2O_2 *via* α-radiolysis of water, which is supported by the observation of studtite and metastudtite upon α,[17] β[18] and γ[19] irradiation of UO_2 surfaces, and the thermodynamic stability has been assessed using high temperature oxide-melt solution calorimetry.[20] For storage in geological repositories, an understanding of how the phase altered products interact with other radionuclides is important.

[a]*School of Chemistry, University of Dublin, Trinity College, Dublin 2, Ireland. E mail: bakerrj@tcd.ie; Fax: +353 1 6712826; Tel: +353 1 8963501*
[b]*Institut für Nukleare Entsorgung (INE), Hermann von Helmholtz Platz, 76344 Eggenstein Leopoldshafen, Germany. E mail: tonya.vitova@kit.edu; Tel: +49 721 608 24024*

†Electronic supplementary information (ESI) available: Powder diffraction data, U s DOS; HR XANES fitting data and vibrational spectra for studtite, meta studtite and schoepite. See DOI: 10.1039/c3dt52437j

Caesium[21] and strontium[22] have both been shown to be sorbed onto studtite, whilst ^{90}Sr, ^{137}Cs, ^{99}Tc, ^{237}Np and ^{239}Pu have been observed to concentrate in metastudtite on the basis of a 2 year immersion study of SNF.[23] Interestingly, ^{241}Am and ^{244}Cm do not concentrate to such a degree. There also appears to be a preference for ^{237}Np incorporation into metastudtite over metaschoepite (6500 ppm and <10 ppm respectively), although batch dissolution studies showed that ^{237}Np is then released into the aqueous phase.[24] We have recently used solid-state electrochemistry to probe the redox properties of studtite and shown that this could oxidise Np(IV) to Np(V) thus allowing a transport mechanism for water soluble neptunium migration.[25] Other possibilities such as substitution of a $\{UO_2\}^{2+}$ fragment for a $\{NpO_2\}^{+}$ fragment also requires a charge balancing step within the mineral structure, whilst recent evidence suggests that interaction of Np containing solutions allow for a direct $\{NpO_2\}^{2+}$ substitution in copper uranyl phosphates.[26]

We have recently initiated a study on the chemical and electrochemical behaviour of some uranyl minerals and we noted that the electronic structure of studtite and metastudtite were different, with a band-gap measured at the absorption edge in the diffuse-reflectance UV-vis spectrum of 3.45 eV and 2.71 eV for studtite and metastudtite, respectively.[25] This is somewhat surprising as only interstitial water molecules (*i.e.* those not directly coordinated to the uranium) are removed in the dehydration, whilst the coordinated water and peroxide do not change, as observed by the similarities in the Raman spectra.[24] In order to understand this unexpected difference we have utilised U–L_3 edge extended X-ray absorption fine structure (EXAFS) and high-energy resolution X-ray absorption near edge structure (HR-XANES) spectroscopic techniques; the latter is a recent development that allows the U unoccupied d and f density of states to be more effectively probed.[27] The experimental results are supported by calculations by the *ab initio* quantum chemical code FEFF9.5.1.[28] In this contribution we report the solid-state characterisation of metastudtite for the first time experimentally and compare the HR-XANES spectra of studtite, metastudtite and schoepite.

Results and discussion

EXAFS study of studtite, metastudtite and schoepite

Whilst schoepite[29] and studtite[30] have been structurally characterised by single crystal X-ray diffraction, there has not been such a determination of the molecular structure of metastudtite. The solid state structure of studtite comprises of infinite chains of uranyl peroxides and a bent U–(O_2)–U dihedral angle. The interstitial water molecules connect two chains by hydrogen bonding. Powder X-ray diffraction data has been reported for studtite,[31] synthetic[32] and naturally occurring metastudtite.[10b] Studtite and metastudtite have been the focus of *ab initio*[33] and DFT studies.[34,35] We have analysed the U–L_3 edge EXAFS spectra of both studtite and metastudtite in order to explore the structural changes around the uranium

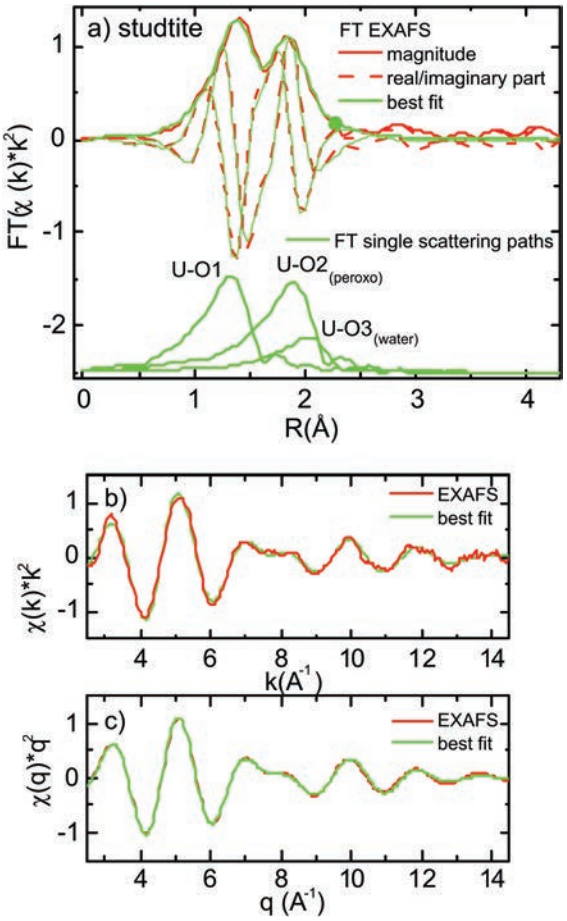

Fig. 1 U L_3 edge Fourier transformed EXAFS and vertically shifted used single scattering paths (a), k^2 weighted (b) and q^2 weighted (c) EXAFS spectra and best fits for studtite.

centres upon removal of the interstitial water molecules. The spectra and best fits are shown in Fig. 1 and 2. The obtained structural data is collected in Table 1 (for numbering scheme see Scheme 1). The U–L_3 edge EXAFS results for studtite compare well for the U O$_{yl}$ and U–O_{peroxo} to the single-crystal X-ray results (for comparison see Table 2). The U–O_{water} is about 0.1 Å longer than that measured by XRD. Such differences are possible due to the sensitivity of the EXAFS spectrum, in contrast to XRD, to structural defects and disorder affecting the average inter-atomic distances and coordination numbers. DFT reports longer distances than obtained from XRD and EXAFS except for the U–O_{water} distance, which is 0.1 Å longer in the EXAFS results. The EXAFS data of metastudtite differ somewhat significantly from the recent computations.[34,35] The EXAFS reports similar U O$_{yl}$ bond length in metastudtite and studtite. This can be confirmed by inspection of the Raman and infrared spectra (Fig. S1 and S2†)[36] of both studtite and metastudtite, as there is no observable difference in either the O–H or U O stretching or bending modes. There is however a small shortening in the U–O_{peroxo} bond length of 0.04 ± 0.01 Å upon dehydration of studtite to metastudtite. Whilst we are unable to measure the O–O bond length

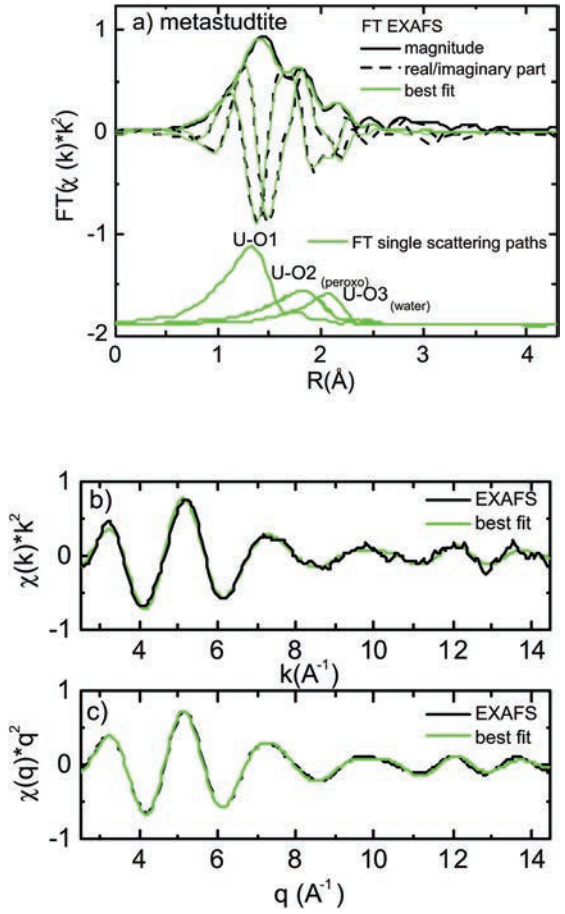

Fig. 2 U L_3 edge Fourier transformed EXAFS and vertically shifted used single scattering paths (a), k^2 weighted (b) and q^2 weighted (c) EXAFS spectra and best fits for metastudtite.

from the EXAFS data, the IR and Raman spectra show no change in the O–O stretching mode, implying that this distance does not change. The U–L_3 edge EXAFS spectrum of schoepite is shown in Fig. 3. The solid-state structure of schoepite has a sheet topology whereby the uranium (oxy)hydroxide sheets are linked to another sheet by hydrogen bonding to interlayer water molecules. The local coordination around the uranium is a pentagonal bipyramid, with the –yl oxygens in

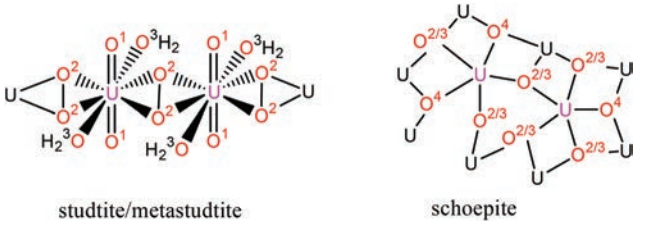

Scheme 1 Schematic of the structures of studtite, metastudtite and schoepite with the numbering scheme (the yl oxygens of schoepite are perpendicular to the page).

Table 2 Bond lengths (Å) for studtite and metastudtite

	Studtite			Metastudtite	
Bond	EXAFS	X ray[30]	DFT[35]	EXAFS	DFT[35]
U═O_{yl}	1.78	1.769	1.83	1.79	1.85 1.80
U O_{peroxo}	2.36	2.365	2.38	2.32	2.39
U O_{water}	2.50	2.395	2.41	2.52	2.42

the apical positions. There are two different uranium centres, one of which is coordinated by 5 μ_3-OH groups and one that has 4 μ_3-O/OH and one μ_2-OH group (Scheme 1). Our data correlates well with previous EXAFS studies,[37] and we can clearly distinguish between O2/O3 and O4. It is also worth noting that structural[38] and *ab initio* calculations[39] on schoepite and metaschoepite show difference in hydrogen bonding upon dehydration.

HR-XANES spectroscopy

Whilst EXAFS gives information on the structure, XANES data provides detailed information on the oxidation state and electronic structure. The experimental and calculated U–L_3 edge HR-XANES spectra of studtite and metastudtite are shown in Fig. 4, along with the calculated U d- and f-DOS of studtite and metastudtite. Energy positions and intensities of the three main features *viz.* pre-edge (A), most intense resonance (white line, WL, B) and post-edge (C), agree reasonably well between experiment and calculation. As previously observed,[27a,c,d] the pre-edge in U(VI)–L_3 HR-XANES spectra mainly describes weak

Table 1 Summary of EXAFS results for studtite, metastudtite and schoepite. From left to right is given: the name of the mineral (Mineral), scattering path (Path), coordination number (N), average U O distance (R(Å)) energy shift of the ionization potential (ΔE(eV)), mean squared atomic displacement/Debye Waller factor (σ^2 (Å^2)), goodness of fit (r factor)

Mineral	Path	N	R (Å)	ΔE (eV)	σ^2 (Å^2)	r factor
Studtite	U O1	2 ± 0.2	1.78 ± 0.01	0.6 ± 0.6	0.003 ± 0.0005	0.01
	U $O2_{(peroxo)}$	4 ± 0.5	2.36 ± 0.01	0.6 ± 0.6	0.004 ± 0.002	0.01
	U $O3_{(water)}$	2	2.5 ± 0.01	0.6 ± 0.6	0.004 ± 0.002	0.01
Metastudtite	U O1	1.7 ± 0.3	1.79 ± 0.01	1 ± 0.9	0.004 ± 0.0007	0.02
	U $O2_{(peroxo)}$	2.0 ± 1.3	2.32 ± 0.01	1 ± 0.9	0.007 ± 0.002	0.02
	U $O2_{(peroxo)}$	2	2.33 ± 0.01	1 ± 0.9	0.007 ± 0.002	0.02
	U $O3_{(water)}$	1.4 ± 0.3	2.52 ± 0.01	1 ± 0.9	0.002 ± 0.0018	0.02
Schoepite	U O1	1.9 ± 0.2	1.77 ± 0.01	1 ± 0.8	0.003 ± 0.0009	0.01
	U O2/3	3.5 ± 1	2.32 ± 0.02	1 ± 0.8	0.013 ± 0.002	0.01
	U O4	2.4 ± 0.6	2.51 ± 0.02	1 ± 0.8	0.008 ± 0.002	0.01

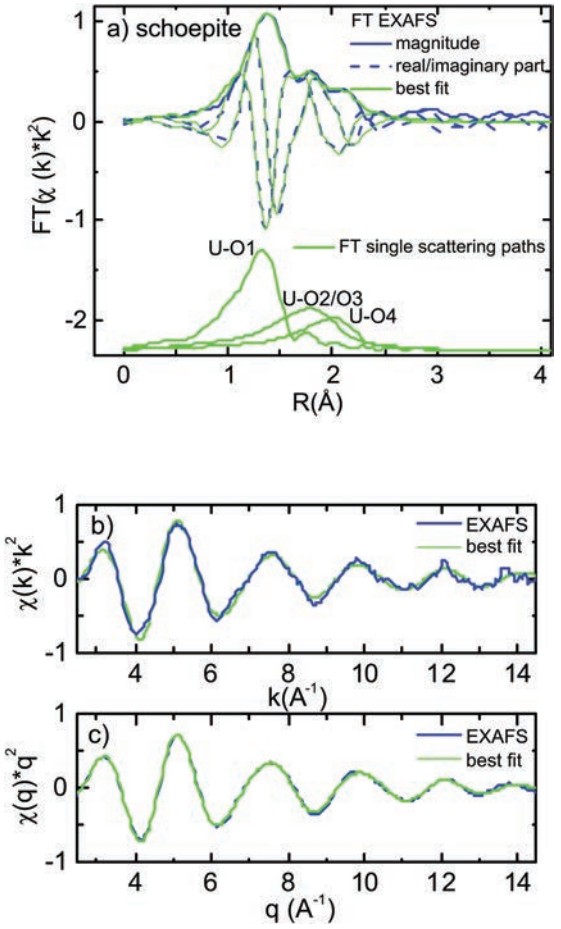

Fig. 3 U L_3 edge Fourier transformed EXAFS and vertically shifted used single scattering paths (a), k^2 weighted (b) and q^2 weighted (c) EXAFS spectra and best fits for schoepite.

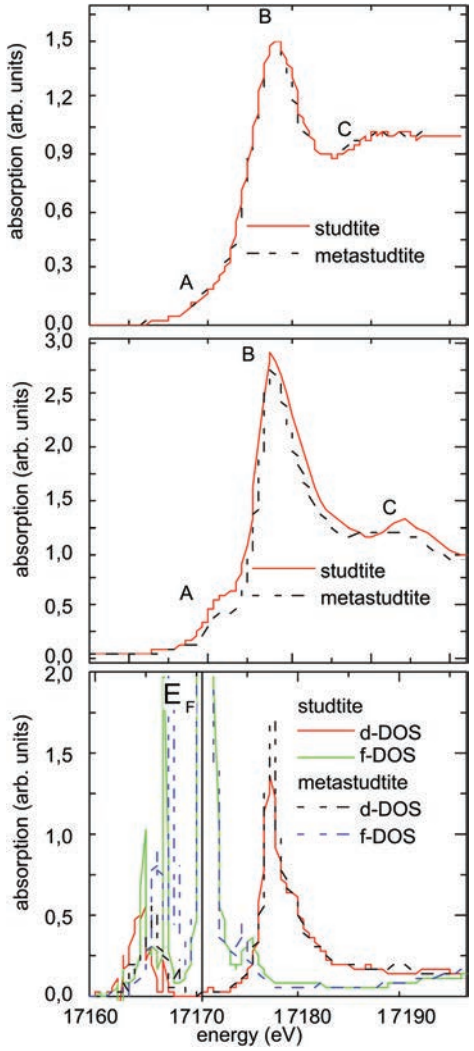

Fig. 4 Experimental (top) and calculated (middle) U L_3 Edge HR XANES spectra and calculated U d and f DOS (bottom) of studtite and meta studtite. The E_F line separates the occupied from the unoccupied DOS.

quadrupole transitions of uranium $2p_{5/2}$ electrons to electronic states with dominating f character. The f-DOS intensity dominates at this energy position, whereas no significant unoccupied s- (shown in Fig. S4†) or d-DOS contribution is visible (Fig. 4 bottom). Note that dipole transitions at this energy position are also possible. The FEFF code is based on the real-space Green's function formalism applied in the Fermi's Golden rule avoiding explicit calculation of the computationally difficult final states. Additionally, relativistic Dirac–Fock approach is used to evaluate the spin–orbit coupling of atomic states and semi-relativistic approximation for scattering and propagation of the photo electron. FEFF calculates the scattering potentials self-consistently within the spherical muffin-tin approximation.[28] This approach might need corrections for small anisotropic systems. The good agreement between experimental and calculated XANES spectra for the crystalline solid state materials investigated herein confirm the validity of the used theoretical approach.[40]

It is known that the energy distance (ΔE) between features B and C (B–C) decreases upon elongation of the U(v/vi)–O_{ax} bonding (R) following the relation $\Delta E \cdot R^2$ = cst typical for all An with –yl type of bonding.[41] Additionally, it has been shown for Np in a theoretical study using the FEFF8.2 code, that B–C weakly decreases by about 0.5 eV for 0.2 Å shortening of the Np(v/vi)–O_{eq} bond length, whereas by 4 eV for 0.08 Å elongation of the Np(v/vi)–O_{ax} bond length.[41] The modelling of the spectra with three pseudo Voigt (PV) profiles and an error function reports 1.3 eV ± 0.1 shorter B–C distance for metastudtite compared to studtite (Table S1, Fig. S5 and S6†) indicating that the 0.01 Å difference of the U–O_{ax} bonds suggested by EXAFS might be indeed present. EXAFS finds 0.04 ± 0.01 Å shorter U–O_{peroxo} for metastudtite compared to studtite, which is unlikely to influence significantly the B–C energy distance.

The occupied O p-DOS and U d- and f-DOS of metastudtite (225 atoms), plotted in Fig. 5, are shifted to higher energies decreasing the band gap of metastudtite by about 1.3 eV compared to studtite (arrow in Fig. 5 middle). By calculating DOS of small studtite and metastudtite atomic clusters with a radius of about 2.6 Å (9 atoms) by varying the U–O_{ax}, O_{peroxo} or O_{water} distances, we found that U–O_{ax} distance has the largest

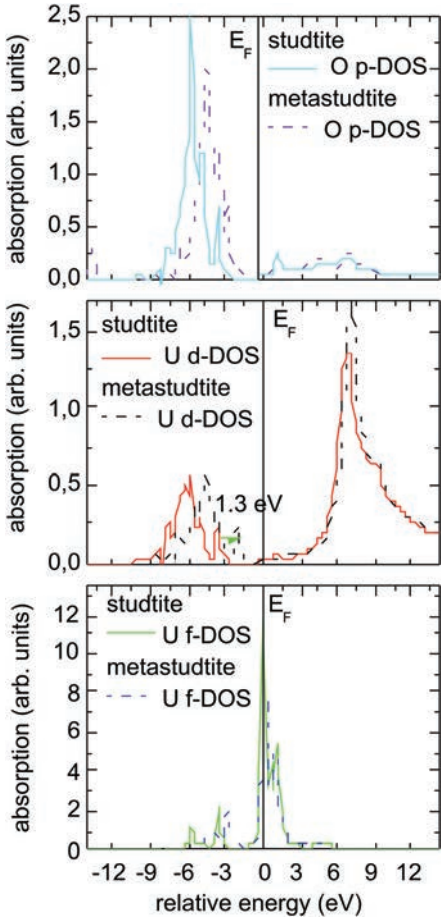

Fig. 5 The O p DOS (top), U d DOS (middle) and f DOS (bottom) of metastudtite. The E_F line separates the occupied from the unoccupied DOS.

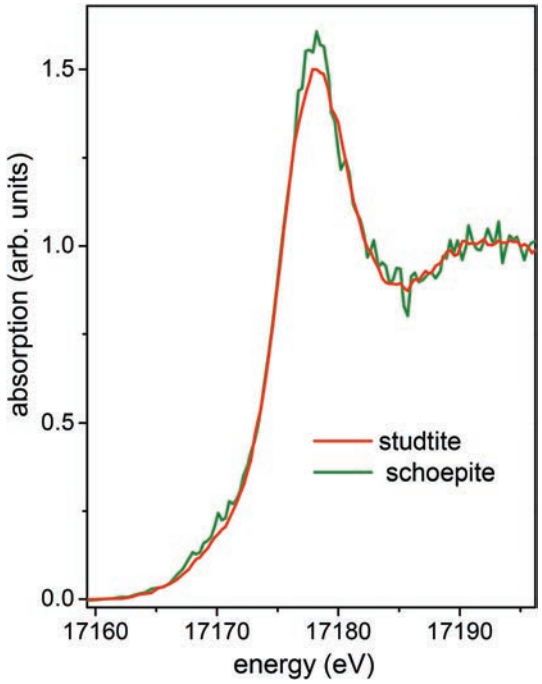

Fig. 6 The experimental U L_3 edge HR XANES of schoepite and studtite.

influence on the reduction of the size of the band gap. For 9 atoms cluster considering distances obtained from the EXAFS analyses, the band gap is reduced by about 0.6 eV for metastudtite compared to studtite. This electronic structural change is in agreement with the difference in the band gaps (0.74 eV) determined by diffuse reflectance spectroscopy.

Therefore, on the basis of the EXAFS and HR-XANES spectra, we can suggest that upon dehydration of studtite the U–O_{peroxo} bond lengths slightly decreases, whilst the U–O_{yl} bond lengths slightly increases, which might decrease the energy gap between the peroxo π type orbitals of the HOMO and the 5f non-bonding orbitals of the LUMO.

The bonding in molecular uranyl peroxides such as $[UO_2(O_2)(H_2O)_3]$ has been the subject of some recent computational studies and shown to have some covalent character by an Atoms-in-Molecules approach,[42] and in the compounds $[UO_2(O_2)_2]^{2-}$ there is increased mixing between the uranium d and peroxo π orbitals.[43] In models of uranyl peroxo clusters, the HOMO has been alternatively described as either comprising of the uranium 6p orbitals overlapping with the peroxo π orbital,[44] or the uranium f_{xyz} orbital overlapping with the peroxo π* orbital; the overlap is enhanced by the bending of the U–(O_2)–U dihedral angle.[45] Therefore in molecular compounds there may be enhanced covalency but in clusters the bonding has been argued as principally ionic with a small amount of covalency.[45] Interestingly, the uranyl–hydroxo interaction is considered to be predominantly ionic,[42,45,46] so a comparison of studtite and schoepite will test the ability of the U–L_3 edge HR-XANES technique to discriminate between small amounts of covalency in these systems. The HR-XANES spectrum of schoepite (Fig. 6) exhibits slightly higher WL and pre-edge intensity compared to the WLs and pre-edge structures of studtite and metastudtite possibly indicating less mixing of metal and ligand atomic orbitals, *i.e.* higher degree of bonding ionicity (see also Fig. S6†). The core-hole lifetime broadening is reduced from 7.4 eV to 4.2 eV in U–L_3 HR-XANES compared to standard XANES;[47] however the broadening affecting the U–L_3 edge spectra is still large, therefore it is not possible to draw accurate conclusions about the bonding difference between schoepite and studtite. Future U–M edge HR-XANES and valence-band inelastic X-ray scattering experiments will reliably probe the U f unoccupied and f and d occupied states and thereby provide additional insights into the nature of bonding in studtite and schoepite.[27c]

Conclusions

We have used EXAFS spectroscopy to compare the structure for studtite and its dehydrated congener metastudtite, which represents the first experimental elucidation of the structure of the latter species. The EXAFS data show that the major structural change upon dehydration is the 0.04 Å shortening of the

$U–O_{peroxo}$ bond length, whereas the $U–O_{yl}$ might be elongated by 0.01 Å. These structural differences might induce a decrease of the HOMO–LUMO energy gap and account for the experimental observations from diffuse reflectance UV-vis spectroscopy. Evaluating the electronic properties for Uranyl peroxo species using more molecular suited theory could provide additional insight in terms of the changes in HOMO–LUMO gap, nature of the transitions and excited states, covalency and bonding structure. Novel spectroscopy techniques such as U–M edge HR-XANES and VB-RIXS are expected to have valuable contribution to the discussion about the nature of the bonding in schoepite and studtite.

Experimental

Schoepite,[48] studtite and metastudtite[32] were prepared as described in the literature and purity was checked by powder X-ray diffraction (Fig. S7–9†). Powder diffraction was performed on a Siemens D500 using a Bragg–Brentano geometry with step size of 0.02° at 16 s each for metastudtite and schoepite and 0.05° at 2.8 s each for studtite. 20 mg from each uranyl compound was ground with cellulose powder (100 mg) and pressed into 1 cm diameter pellets of homogeneous character. The EXAFS and HR-XANES measurements were performed at the INE-Beamline, ANKA synchrotron radiation facility, Karlsuhe, Germany. The primary X-ray beam was vertically collimated by a cylindrically bent Rh coated mirror, monochromatized by a Ge(422) double crystal monochromator and focused by a toroidal double-focusing Rh-coated mirror to $500 \times 500\ \mu m^2$ onto the sample. For detailed description of the INE-Beamline see ref. 49.

The initial alignment of the multi-analyzer crystals spectrometer (MAC-spectrometer) was performed by using the elastically scattered from a Teflon sample incident X-rays with energy of 9570.4 eV diffracted by five Ge(555) analyzer crystals (Saint-Gobain Crystals, France) set at 82.55° Bragg angle. The experimental energy resolution was estimated by measuring the full-width at half maximum of the elastically scattered peak. The obtained value is 0.1 eV larger than the calculated value 1.9 eV and implies minor deviations of the positions of the sample, crystal and/or detector from the ideal Rowland circle geometry and/or source size effects.

The emitted fluorescence from the uranium minerals was diffracted by the 5 Ge(777) analyzer crystals and focused on a SDD VORTEX. The sample, crystals and detector were positioned on a Rowland circle in the vertical plane with diameter of 1 m equal to the bending radius of the spherically bent analyzer crystals. The multi analyser crystal spectrometer (MAC-Spectrometer) was set at the maximum of the U Lα1 emission line (77.39° Bragg angle), whereas the primary energy was scanned to obtain U L_3 edge (17 166 eV) HR-XANES spectra. It was not possible to measure the experimental energy resolution at this photon energy due to the low elastic scattering cross section.

The oscillating $\chi(k)$ (EXAFS) part of the X-ray absorption spectroscopy (XAS) spectrum was extracted, Fourier transformed (FT) and modelled by using the ATHENA and ARTEMIS programs, respectively, parts of the IFFEFIT program package.[50] The single scattering paths were generated with the FEFF8.2 code[51] by using the structural models reported in ref. 30 and 35. The $\chi(k)$ spectra within 2.5–14.5 $Å^{-1}$ range were weighted by $k = 1$, 2 or 3. Hanning windows with sills equal to 2 ($dk = 2$) were used. The fit was performed in R space for 1.07–2.38 Å range. For each shell, the coordination number was first fixed and the change in distance and the Debye Waller (DW) factors were varied. In a second step, the coordination number was varied simultaneously with the obtained from the first step DW factors, whereas the change in distance was fixed. The number of variables was kept always half or less the number of independent data points. The obtained goodness of fit (r factor) reports 1% ($r = 0.01$, studtite, schoepite) or 2% ($r = 0.02$, metastudtite) difference between data and model.

The background subtraction and normalization of the XANES part of the experimental spectra was performed with ATHENA. The HR-XANES and angular momentum projected density of states (DOS) were calculated by the FEFF9.5.1 *ab initio* quantum chemical theoretical code based on the multiple scattering theory.[28] The scattering potentials were calculated on a cluster of 225 or 9 atoms by including the U f states in the self-consistent loop (FMS, SCF and UNFREEZEF cards).[27c] Final state rule approximation was used to account for core-hole effects (default). The core-hole lifetime broadening was reduced by 2.8 eV and the Fermi energy was shifted by 1 eV to lower energies. Electronic transitions to 5f states were allowed (MULTIPOLE card). Hedin–Lundqvist exchange correlation potential was used.

Acknowledgements

RJB and AW thank IRCSET for funding through the EMBARK initiative. We acknowledge the Helmholtz Association of German Research Centres for the VH-NG-734 grant. We acknowledge Synchrotron Light Source ANKA for provision of instruments at their beamlines. COST action CM1006 EUFEN is also acknowledged.

Notes and references

1 W. E. Falck and K.-F. Nilsson, Geological disposal of radioactive waste: moving towards implementation, *Joint Research Centre Reference Report*, EUR23925, 2009.

2 R. J. Baker, *Coord. Chem. Rev.*, 2013, DOI: 10.1016/j.ccr.2013.10.004.

3 (*a*) R. J. Finch, E. C. Buck, P. A. Finn and J. K. Bates, *Mater. Res. Soc. Symp. Proc.*, 1999, **556**, 431; (*b*) P. A. Finn, J. C. Hoh, S. F. Wolf, S. A. Slater and J. K. Bates, *Radiochim. Acta*, 1996, **74**, 65.

4 (*a*) D. J. Wronkiewicz, J. K. Bates, S. F. Wolf and E. C. Buck, *J. Nucl. Mater.*, 1996, **238**, 78; (*b*) D. J. Wronkiewicz, J. K. Bates, T. J. Gerding, E. Veleckis and B. S. Tani, *J. Nucl. Mater.*, 1992, **190**, 107.

5 (*a*) B. Hanson, B. McNamara, E. Buck, J. Friese, E. Jenson and K. Krupka, *Radiochim. Acta*, 2005, **93**, 159; (*b*) B. McNamara, E. Buck and B. Hanson, *Mater. Res. Soc. Symp. Proc.*, 2002, **757**, 401.

6 (*a*) K.-W. Kim, J.-T. Hyun, K.-Y. Lee, E.-H. Lee, K.-W. Lee, K.-C. Song and J.-K. Moon, *J. Hazard. Mater.*, 2011, **193**, 52; (*b*) F. Clarens, J. de Pablo, I. Casas, J. Giménez, M. Rovira, J. Merino, E. Cera, J. Bruno, J. Quiñones and A. Martínez-Esparza, *J. Nucl. Mater.*, 2005, **345**, 225; (*c*) F. Clarens, J. de Pablo, I. Díez, I. Casas, J. Giménez and M. Rovira, *Environ. Sci. Technol.*, 2004, **38**, 6656; (*d*) M. Amme, B. Renker, B. Schmid, M. P. Feth, H. Bertagnolli and W. Döbelin, *J. Nucl. Mater.*, 2002, **306**, 202; (*e*) P. Diaz-Arocas, J. Quinones, C. Maffiotte, J. Serrano, J. Garcia, J. R. Almazan and J. Esteban, *Mater. Res. Soc. Symp. Proc.*, 1995, **353**, 641.

7 (*a*) T. Z. Forbes, P. Horan, T. Devine, D. McInnis and P. C. Burns, *Am. Mineral.*, 2011, **96**, 202; (*b*) R. J. Finch and R. C. Ewing, *Mater. Res. Soc. Symp. Proc.*, 1994, **333**, 625.

8 J. Abrefah, S. Marschmann and E. D. Jenson, PNNL-11806, Pacific Northwest National Laboratory, Richland, WA, 1998.

9 B. E. Burakov, E. E. Strykanova and E. B. Anderson, *Mater. Res. Soc. Symp. Proc.*, 1997, **465**, 1309.

10 (*a*) J. Čejka, J. Sejkora and M. Deliens, *Neues Jahrb. Mineral., Monatsh.*, 1996, 125; (*b*) M. Deliens and P. Piret, *Am. Mineral.*, 1983, **68**, 456; (*c*) K. Walenta, *Am. Mineral.*, 1974, **59**, 166.

11 G. S. Goff, L. F. Brodnax, M. R. Cisneros, S. M. Peper, S. E. Field, B. L. Scoft and W. H. Runde, *Inorg. Chem.*, 2008, **47**, 1984.

12 S. Meca, A. Martinez-Torrents, V. Marti, J. Gimenez, I. Casas and J. de Pablo, *Dalton Trans.*, 2011, **40**, 7976.

13 (*a*) P. L. Zanonato, P. Di Bernardo and I. Grenthe, *Dalton Trans.*, 2012, **41**, 3380; (*b*) A. Martínez-Torrents, S. Meca, N. Baumann, V. Martí, J. Giménez, J. de Pablo and I. Casas, *Polyhedron*, 2013, **55**, 92.

14 M. Nyman, M. A. Rodriguez and C. F. Campana, *Inorg. Chem.*, 2010, **49**, 7748.

15 For recent reviews see: (*a*) P. C. Burns, *Mineral. Mag.*, 2011, **75**, 1; (*b*) R. J. Baker, *Chem.–Eur. J.*, 2012, **18**, 16258.

16 C. R. Armstrong, M. Nyman, T. Shvareva, G. E. Sigmon, P. C. Burns and A. Navrotskya, *Proc. Natl. Acad. Sci. U. S. A.*, 2012, **109**, 1874.

17 G. Sattonnay, C. Ardois, C. Corbel, J. F. Lucchini, M.-F. Barthe, F. Garrido and D. Gosset, *J. Nucl. Mater.*, 2001, **288**, 11.

18 F. Clarens, J. Giménez, J. de Pablo, I. Casas, M. Rovira, J. Dies, J. Quiñones and A. Martínez-Esparza, *Radiochim. Acta*, 2005, **93**, 533.

19 C. Jegou, B. Muzeau, V. Broudic, S. Peuget, A. Poulesquen, D. Roudil and C. Corbel, *J. Nucl. Mater.*, 2005, **341**, 62.

20 K.-A. Hughes Kubatko, K. B. Helean, A. Navrotsky and P. C. Burns, *Science*, 2003, **302**, 1191.

21 J. Giménez, X. Martínez-Lladó, M. Rovira, J. de Pablo, I. Casas, R. Sureda and A. Martínez-Esparza, *Radiochim. Acta*, 2010, **98**, 479.

22 R. Sureda, X. Martínez-Lladó, M. Rovira, J. de Pablo, I. Casasa and J. Giménez, *J. Hazard. Mater.*, 2010, **181**, 881.

23 B. McNamara, B. Hanson, E. Buck and C. Soderquist, *Radiochim. Acta*, 2005, **83**, 169.

24 M. Douglas, S. B. Clark, J. I. Friese, B. W. Arey, E. C. Buck and B. D. Hanson, *Environ. Sci. Technol.*, 2005, **39**, 4117.

25 C. Mallon, A. Walshe, R. J. Forster, T. E. Keyes and R. J. Baker, *Inorg. Chem.*, 2012, **51**, 8509.

26 N. A. Meredith, M. J. Polinski, J. N. Cross, E. M. Villa, A. Simonetti and T. E. Albrecht-Schmitt, *Cryst. Growth Des.*, 2013, **13**, 386.

27 (*a*) T. Vitova, K. O. Kvashnina, G. Nocton, G. Sukharina, M. A. Denecke, S. M. Butorin, M. Mazzanti, R. Caciuffo, A. Soldatov, T. Behrends and H. Geckeis, *Phys. Rev. B: Condens. Matter*, 2010, **82**, 235118; (*b*) G. B. Sukharina, A. V. Soldatov, O. N. Batuk and M. A. Denecke, *Nucl. Instrum. Methods Phys. Res., Sect. A*, 2009, **603**, 125; (*c*) T. Vitova, M. A. Denecke, J. Göttlicher, K. Jorissen, J. J. Kas, K. Kvashnina, T. Prüßmann, J. J. Rehr and J. Rothe, *J. Phys.: Conf. Ser.*, 2013, **430**, 012117; (*d*) M. A. Denecke, M. Borchert, R. G. Denning, W. De Nolf, G. Falkenberg, S. Honing, M. Klinkenberg, K. Kvashnina, S. Neumeier, J. Patommel, T. Petersmann, T. Pruesmann, S. Ritter, C. Schroer, S. Stephan, J. Villanova, T. Vitova and G. Wellenreuther, *MRS Proc.*, 2012, **1444**, 12.

28 J. J. Rehr, J. J. Kas, F. D. Vila, M. P. Prange and K. Jorissen, *Phys. Chem. Chem. Phys.*, 2010, **12**, 5503.

29 (*a*) R. J. Finch, M. A. Cooper, F. C. Hawthorne and R. C. Ewing, *Can. Mineral.*, 1996, **34**, 1071; (*b*) R. J. Finch, F. C. Hawthorne and R. C. Ewing, *Can. Mineral.*, 1998, **36**, 831.

30 P. C. Burns and K.-A. Hugues, *Am. Mineral.*, 2003, **88**, 1165.

31 S. Planteur, M. Bertrand, E. Plasari, B. Courtaud and J.-P. Gaillard, *CrystEngComm*, 2013, **15**, 2305.

32 P. C. Debets, *J. Inorg. Nucl. Chem.*, 1963, **25**, 727.

33 S. Ostanin and P. Zeller, *Phys. Rev. B: Condens. Matter*, 2007, **75**, 073101.

34 L. C. Schuller, R. C. Ewing and U. Becker, *Am. Mineral.*, 2010, **95**, 1151.

35 P. F. Weck, E. Kim, C. F. Jové-Colón and D. C. Sassani, *Dalton Trans.*, 2012, **41**, 9748.

36 S. Bastians, G. Crump, W. P. Griffith and R. Withnall, *J. Raman Spectrosc.*, 2004, **35**, 726.

37 (*a*) P. G. Allen, D. K. Shuh, J. J. Bucher, N. M. Edelstein, C. E. A. Palmer, R. J. Silva, S. N. Nguyen, L. N. Márquez and E. A. Hudson, *Radiochim. Acta*, 1996, **75**, 47; (*b*) S. El Aamrani, J. Giménez, M. Rovira, F. Seco, M. Grivé, J. Bruno, L. Duro and J. de Pablo, *Appl. Surf. Sci.*, 2007, **253**, 8794.

38 M. T. Weller, M. E. Light and T. Gelbrich, *Acta. Crystallogr., Sect. B: Struct. Sci.*, 2000, **56**, 577.

39 S. Ostanin and P. Zeller, *J. Phys.: Condens. Matter*, 2007, **19**, 246108.
40 See also: S. Heathman, J.-P. Rueff, L. Simonelli, M. A. Denecke, J.-C. Griveau, R. Caciuffo and G. H. Lander, *Phys. Rev. B: Condens. Matter*, 2010, **82**, 201103(R).
41 (*a*) C. Den Auwer, E. Simoni, S. Conradson and C. Madic, *Eur. J. Inorg. Chem.*, 2003, 3843; (*b*) J. Petiau, G. Calas and D. Petit-Maire, *Phys. Rev. B: Condens. Matter*, 1986, **34**, 7350; (*c*) E. A. Hudson, *Phys. Rev. B: Condens. Matter*, 1996, **54**, 156; (*d*) A. L. Ankudinov, *Phys. Rev. B: Condens. Matter*, 1998, **57**, 7518.
42 V. Vallet, U. Wahlgren and I. Grenthe, *J. Phys. Chem. A*, 2012, **116**, 12373.
43 S. O. Odoh and G. Schreckenbach, *Inorg. Chem.*, 2013, **52**, 5590.
44 B. Vlaisavljevich, L. Gagliardi and P. C. Burns, *J. Am. Chem. Soc.*, 2010, **132**, 14503.
45 P. Miró, S. Pierrefixe, M. Gicquel, A. Gil and C. Bo, *J. Am. Chem. Soc.*, 2010, **132**, 17787.
46 (*a*) K. I. M. Ingram, L. J. L. Häller and N. Kaltsoyannis, *Dalton Trans.*, 2006, 2403; (*b*) S. Tsushima, *Dalton Trans.*, 2011, **40**, 6732.
47 P. Glatzel, T.-C. Weng, K. Kvashnina, J. Swarbrick, M. Sikora, E. Gallo, N. Smolentsev and R. A. Mori, *J. Electron Spectrosc. Relat. Phenom.*, 2013, **188**, 17.
48 O. V. Nipruk, A. V. Knyazev, G. N. Chernorukov and Y. P. Pykhova, *Radiochemistry*, 2011, **53**, 146.
49 J. Rothe, S. Butorin, K. Dardenne, M. A. Denecke, B. Kienzler, M. Löble, V. Metz, A. Seibert, M. Steppert, T. Vitova, C. Walther and H. Geckeis, *Rev. Sci. Instrum.*, 2012, **83**, 043105.
50 B. Ravel and M. Newville, *J. Synchrotron Radiat.*, 2005, **12**, 537.
51 J. J. Rehr and R. C. Albers, *Rev. Mod. Phys.*, 2000, **72**, 621.

Karlsruher Institut für Technologie

OPEN ACCESS

Repository KITopen

Dies ist ein Postprint/begutachtetes Manuskript.

Empfohlene Zitierung:

Walshe, A.; Prüßmann, T.; Vitova, T.; Baker, R. J.
An EXAFS and HR-XANES study of the uranyl peroxides $[UO_2(\eta^2\text{-}O_2)(H_2O)_2].nH_2O$ (n = 0, 2) and uranyl (oxy)hydroxide $[(UO_2)_4O(OH)_6].6H_2O$
2014. Dalton transactions, 43, 4400–4407.
doi:10.5445/IR/110098705

Zitierung der Originalveröffentlichung:

Walshe, A.; Prüßmann, T.; Vitova, T.; Baker, R. J.
An EXAFS and HR-XANES study of the uranyl peroxides $[UO_2(\eta^2\text{-}O_2)(H_2O)_2].nH_2O$ (n = 0, 2) and uranyl (oxy)hydroxide $[(UO_2)_4O(OH)_6].6H_2O$
2014. Dalton transactions, 43, 4400–4407.
doi:10.1039/C3DT52437J

Lizenzinformationen: KITopen-Lizenz